Expanding the bandwidth of fluorescence-detected two-dimensional electronic spectroscopy using a broadband continuum probe pulse pair

STEPHANIE SANDERS,[1,†] MUYI ZHANG,[1,†] ARIBA JAVED[1] AND JENNIFER P. OGILVIE[1,*]

[1]*Department of Physics, University of Michigan, 450 Church St, Ann Arbor, MI 48109, USA*
[†]*Equal author contributions*
**jogilvie@umich.edu*

Abstract: We demonstrate fluorescence-detected two-dimensional electronic spectroscopy (F-2DES) with a broadband, continuum probe pulse pair in the pump-probe geometry. The approach combines a pump pulse pair generated by an acousto-optic pulse-shaper with precise control of the relative pump pulse phase and time delay with a broadband, continuum probe pulse pair created using the Translating Wedge-based Identical pulses eNcoding System (TWINS). The continuum probe expands the spectral range of the detection axis and lengthens the waiting times that can be accessed in comparison to implementations of F-2DES using a single pulse-shaper. We employ phase-cycling of the pump pulse pair and take advantage of the separation of signals in the frequency domain to isolate rephasing and non-rephasing signals and optimize the signal-to-noise ratio. As proof of principle, we demonstrate broadband F-2DES on a laser dye and bacteriochlorophyll *a*.

1. Introduction

Two-dimensional electronic spectroscopy (2DES) is a powerful approach for studying excitonic structure and ultrafast dynamics in a wide range of systems[1, 2] including natural [3-8] and artificial [9, 10] light-harvesting systems, semiconductors,[11-13] and solar cell materials. [14, 15] Two-color[16] and continuum probe[17] variations of 2DES are particularly useful for studying systems with large spectral congestion such as photosynthetic reaction centers, where cross-peaks can help disentangle excitonic structure and dynamics. [5, 18-21] However, the cross-peak regions of 2DES spectra are often dominated by excited state absorption (ESA), the signal corresponding to the increase in absorption in the singly-excited state, which obscures the ground state bleach (GSB), the signal corresponding to the decrease in absorption in the ground state, and stimulated emission (SE) signals.

Fluorescence-detected 2DES (F-2DES) has garnered recent interest due to the sensitivity of fluorescence and its compatibility with microscopy due to the ease with which spectral filtering enables a collinear beam geometry. Multiple methods for F-2DES have been implemented [22-26] to study small molecular systems, [26-28] DNA, [29] and light-harvesting complexes. [30, 31] In F-2DES, an additional pulse projects the coherent 2DES signal onto a fluorescent population. The addition of a fourth pulse results in two ESA signals with opposite signs.[27] Depending on the relative fluorescence quantum yield of the singly and doubly excited states, the ESA signals will fully or partially cancel,[27, 32, 33] which may offer an advantage for studying systems in which the coherent 2DES spectra are dominated by ESA. The relative advantages and disadvantages of coherent 2DES and F-2DES are still being established and appear to be system and question-dependent.[34] In coherent 2DES the signal is emitted on an ultrafast timescale determined by the dephasing of the optical coherence, while in F-2DES the excited state emits the detected fluorescence on a ~ns time scale. The long-lived nature of the excited states in F-2DES allows for additional processes to occur that can strongly influence the F-2DES signal. These include exciton-exciton annihilation in multichromophoric

systems [28, 30, 31, 35] and Auger recombination in quantum dots,[36-38] which give rise to dominant cross-peaks in F-2DES spectra. In general, action-detected 2D spectroscopies such as F-2DES and photocurrent-detected 2D are susceptible to nonlinearities in the detection process [39] and incoherent mixing of linear signals [40] that can obscure the nonlinear signal of interest. [34, 41, 42]

The most commonly-used approach to F-2DES, pioneered by Marcus and coworkers, employs two Mach-Zehnder (MZ) interferometers where the phase of each arm is modulated at a unique acousto-optic frequency. [23, 26, 43, 44] The nonlinear signals of interest are then detected at linear combinations of the applied frequencies. The phase-modulation method works well with high repetition rate lasers and offers high signal-to-noise ratios with short data collection times. We have shown that phase-modulation can be used for spatially-resolved F-2DES studies of photosynthetic bacteria.[30] Due to the high repetition rate of the laser excitation that is typically used in phase-modulated F-2DES, this method is less suitable for studying systems with long-lived excited states. Other implementations of F-2DES have employed pulse-shapers with kHz laser sources, making them more suitable for such studies. [24, 25] These methods build on implementations of coherent 2DES that employed pulse-shapers to create the pump pulse pair.[16, 17, 45] Instead of using a separate probe pulse, a single pulse-shaper is used to create all four pulses for the F-2DES experiment,[24] utilizing phase-cycling to extract the nonlinear signals of interest.[46] The pulse-shaping approach has also been used in spatially-resolved F-2DES measurements.[47] A limitation of these methods is the limited bandwidth throughput of the acousto-optic crystals used for phase-modulation/pulse-shaping. In addition, the maximum waiting time delay for the pulse-shaping method is limited to short delays determined by the characteristics of the pulse-shaper (typically ~picoseconds).

To circumvent the bandwidth limitations of the acousto-optic crystals and expand the detection spectral range for F-2DES, we sought a method for generating phase stable pulse pairs in the visible. Cerullo and coworkers developed the Translating Wedge-based Identical pulses eNcoding System (TWINS) interferometer, which exploits birefringence to generate collinear, phase-locked ultrashort pulse pairs with a controllable time delay.[48, 49] Featuring interferometric phase stability, broad spectral acceptance, high time resolution and reproducibility, the TWINS interferometer has been applied in spectroscopy and imaging from the ultraviolet to the infrared.[49-52] In particular, its high throughput over a broad bandwidth makes it a great fit for broadband applications. Here we combine our previous pulse-shaping-based approach that employed the Dazzler pulse-shaper [16, 17] in the pump-probe geometry with continuum probe pulse pair generated by TWINS to expand the bandwidth of F-2DES and enable long waiting-time measurements. We refer to this hybrid TWINS-Dazzler approach to F-2DES as TWIZZLER. We demonstrate TWIZZLER on a laser dye (IR144) and bacteriochlorophyll *a*.

2. Experiment

2.1 Experimental setup

An overview of the TWIZZLER setup is shown in Figure 1. Briefly, a Ti:Sapphire regenerative amplifier (Spectra Physics Spitfire Pro) produces 4 mJ, 35 fs pulses centered around 800 nm at 1 kHz repetition rate. A portion of the output light (1.7 mJ) is used to pump a home-built degenerate optical parametric amplifier (DOPA), [53] generating near-infrared pulses between 680-920 nm. For the pump pulses, the DOPA output is partially compressed with chirped mirrors (CM) and coupled into an acousto-optic pulse-shaper (Dazzler, Fastlite). The Dazzler compresses the pump pulse to ~18 fs and creates a pulse pair (pulses 1 and 2) with controllable time delay (t_1) and relative phase ($\varphi_{21} = \varphi_2 - \varphi_1$). Additionally, we apply a time dependent spectral phase to scan t_1 in the partially rotating frame. [16, 54] The pump pulse pair travels through a delay stage to scan the waiting time delay (T) and is picked off to be parallel to the probe beam. The pump polarization is controlled using a half-wave plate (HWP, Thorlabs

AHWP05M-980) and a polarizer (Pol, Thorlabs LPVIS100-MP2). For the probe pulses, a portion of the 1300 nm pulse generated in the first two stages of the DOPA is picked off and focused into a Yttrium Aluminum Garnet (YAG, 4 mm, Newlight) crystal, producing a broadband white light continuum with a spectrum extending down to 550 nm. Short-pass filters remove residual near-infrared wavelengths. After collimation, the white light continuum is partially compressed by CMs and fed into the TWINS interferometer to generate the probe pulse pair (pulses 3 and 4) with controllable time delay (t_3). A broadband half-wave plate (HWP, Thorlabs AHWP05M-600) is employed to maximize the throughput of the TWINS by rotating the input polarization of the continuum to 45°.

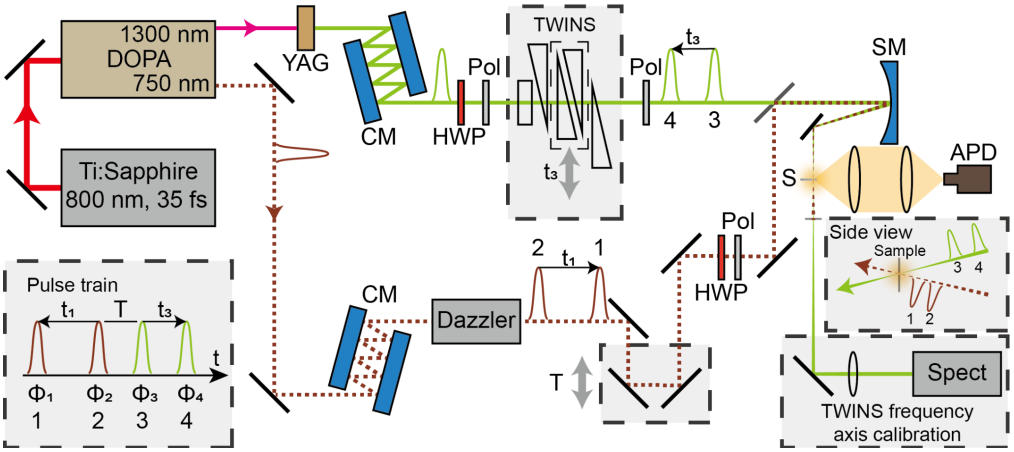

Fig. 1. TWIZZLER experimental setup. The pulse-shaper (Dazzler) generates the pump pulse pair (pulses 1 and 2) with controllable time delay (t_1) and relative phase (φ_{21}), while the TWINS generates the broadband continuum probe pulse pair (pulses 3 and 4) with controllable time delay (t_3). Both beams are focused to the sample (S) with a spherical mirror (SM) in the pump-probe geometry. The fluorescence signal is collected in the 90-degree detection geometry. CM: chirped mirrors. HWP: half-wave plate. Pol: polarizer. APD: avalanche photodiode. Spect: spectrometer.

The working principle of TWINS has been previously reported.[48] Briefly, it is composed of a birefringent plate (α-BBO, 12x12x4 mm, Shalom EO) and two sets of birefringent wedge pairs (α-BBO, 30x12x4.2(0.5) mm, Shalom EO) that are translated to vary the thickness of the material in the beam path. When a light pulse traverses a uniaxial birefringent material, the ordinary and extraordinary polarization components travel with different group velocities. Therefore, the relative time delay between two orthogonally polarized pulses can be scanned by continuously varying the thickness of the material (*i.e.,* translating the wedge pair). The TWINS interferometer has previously been used to generate the pump pulse pair for 2D spectroscopy experiments, where pulse 1 is scanned and pulse 2 is stationary to ensure a constant T delay.[48] However, in our setup, the TWINS interferometer is used to generate the probe pulse pair. We thus require pulse 4 to arrive later than pulse 3 so that the waiting time delay (T) between pulses 2 and 3 is kept constant while scanning t_3. To ensure the correct time ordering, the birefringent plate we use in the TWINS interferometer is comparable in thickness to the wedges (4 mm thick vs 4.2 mm). Both pulses are delayed as a result, but pulse 4 is delayed farther compared to pulse 3 due to birefringence, reversing the time ordering of the pulse pair. Pulses 3 and 4 are recombined after the TWINS interferometer by projecting onto the 45° polarization direction with a polarizer (Pol, Moxtek, PFU04C).

Both the pump and probe pulses are focused onto the sample (S) with a spherical mirror (SM, f=150 mm) in the pump-probe geometry. The pump and probe pulses are laterally overlapped but vertically displaced, with the probe above the pump as displayed in the inset (Side view) of Figure 1. Combining the beams in this manner results in less power loss for the

continuum probe compared with a fully collinear geometry. At the sample position, both the pump and probe spot sizes are ~50 μm with the pump slightly larger than the probe. For the measurements we report here, the pump energy at the sample was 3.1 nJ and 8.8 nJ for IR144 and bacteriochlorophyll *a* respectively, whereas the probe energy was 0.5 nJ. For the IR144 experiments, the pump polarization was rotated 45° relative to the probe and the sample was in a 1 mm pathlength cuvette. For the bacteriochlorophyll *a* experiments, the pump polarization was set parallel to the probe and the sample was flowed through a 0.4 mm square capillary tube with a peristaltic pump to prevent photobleaching. The fluorescence signals were collected in the 90-degree detection geometry using a lens (f = 60 mm, diameter = 2"). Then, the signal was focused onto a photodiode (Femto, OE-200 or Hamamatsu, C12703-01) with a lens (f = 175mm). Long-pass and neutral density filters were used to block scattered laser light and reduce the signal level to the linear regime of the detector, respectively. The signal was fed into a Boxcar Integrator (Stanford Research Systems, SR250) and the integrated signal was read out with a data acquisition card (National Instruments, PCIe-6321) triggered via the Dazzler.

2.2 Data collection scheme

In F-2DES, the third-order polarization, $\hat{P}^{(3)}(t_1, T, t_3)$, is projected onto an excited electronic state that can undergo fluorescence by interaction with a 4th pulse. The measured signal can be broken into three main contributions: the linear fluorescence from the pump pulses, the linear fluorescence from the probe pulses, and the nonlinear fluorescence-detected pump-probe and F-2DES signals. The emitted fluorescence contains the phase information encoded by the light-matter interactions, such that the phases of the rephasing and non-rephasing signals are given by $\varphi_R = -\varphi_1 + \varphi_2 + \varphi_3 - \varphi_4$ and $\varphi_{NR} = \varphi_1 - \varphi_2 + \varphi_3 - \varphi_4$ respectively. Typically, the rephasing and non-rephasing signals in F-2DES are separated from the linear fluorescence signals and the pump-probe signals through phase-cycling [22, 24, 25] or phase-modulation. [23, 27, 30, 43] Here we use a combination of phase-cycling and frequency filtering. Phase-cycling of the pump pulses in the fully or partially rotating frame is readily implemented with the Dazzler. The TWINS interferometer operates in the partially rotating frame, but does not provide control over the relative carrier envelope phase for pulses 3 and 4 (φ_3 and φ_4). Thus phase-cycling alone cannot isolate the signals of interest. However, the linear and nonlinear signals have different frequency dependence during the t_1 and t_3 coherence times. The nonlinear signals are not well separated from the linear fluorescence from the probe because we operate close to the fully rotating frame to minimize the number of samples in t_1. To remove the contribution from the linear fluorescence of the probe, we employed 0-π phase-cycling. The linear fluorescence excitation signal from the probe pulse pair can be obtained by summing of the measurements with the two phases: $S_{Lin,probe}(t_1, T, t_3) = S_{\varphi_{21}=0}(t_1, T, t_3) + S_{\varphi_{21}=\pi}(t_1, T, t_3)$. The difference between the measurements removes the linear fluorescence signal from the probe, leaving the sum of the nonlinear signals and the linear fluorescence signal from the pump pulse pair: $S_{\varphi_{21}=0}(t_1, T, t_3) - S_{\varphi_{21}=\pi}(t_1, T, t_3) = S_{NL+Lin,pumps}(t_1, T, t_3)$. The linear fluorescence signal from the pump pulse pair can be removed via filtering in the frequency domain.

To collect all the required combinations of t_1 and t_3 we continuously scan t_3 with the TWINS interferometer while rapidly and repeatedly stepping through t_1 as seen in the bottom panel of Figure 2. The data is collected while the TWINS stage is scanned in both the forward and backward direction to increase the efficiency of data collection. Zooming on the first iteration of t_1 step scan (top panel of Figure 2), we collect the two relative pump phases (0, π) for each t_1 delay while rapidly scanning t_3. The pulse-shaper is synchronized with the data collection so there is no ambiguity in the t_1 delay and relative pump phase of each shot. However, since the TWINS stage runs continuously, the two phase measurements for each t_1

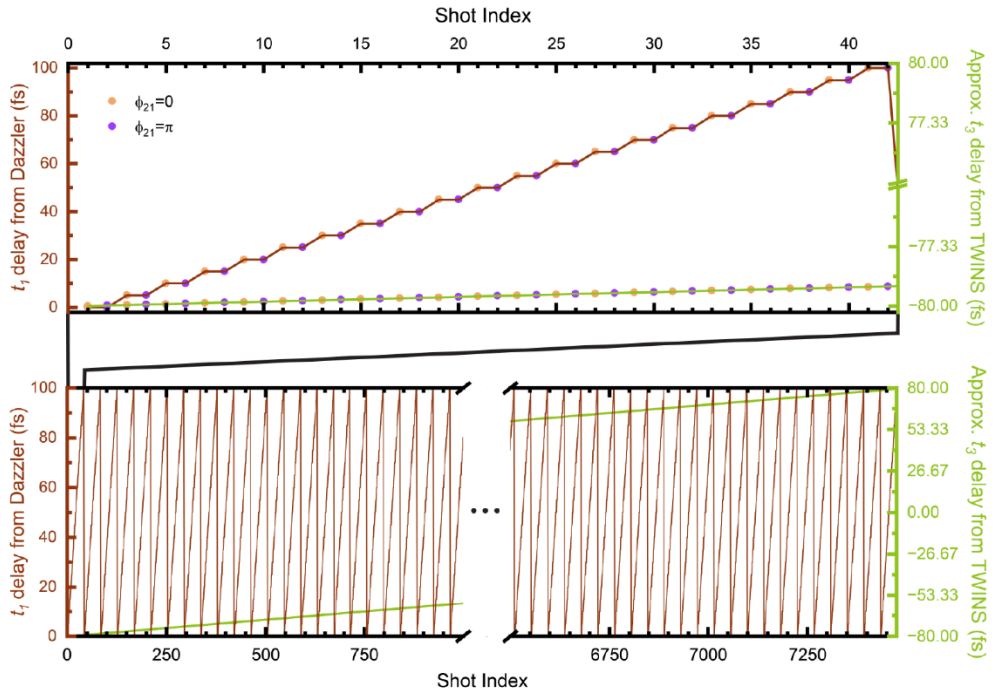

Fig. 2. Phase cycling of the pump pulses while stepping the t_1 delays and scanning the t_3 delays during the first scan through of the t_1 delays (top). Scanning scheme where the t_1 delays are rapidly stepped through using the Dazzler and t_3 delays are continuously scanned using the TWINS. Note the delays from the TWINS is approximate and differs slightly for every wavelength.

delay have slightly different t_3 delays. For our scanning speed of 0.48 mm/s, the spread of t_3 delays was ~1 fs, which was corrected by interpolating the data onto a uniform set of t_3 delays.

In 2D experiments, the TWINS scanning speed and the number of shots to collect in each scan are chosen to satisfy the Nyquist sampling criteria. To minimize the effects of laser noise we collect the (t_1, t_3) time points required for the F-2D scan as quickly as possible while staying above the Nyquist sampling rate. We first determine the range of the t_1 scan and the number of t_1 delays to step through. The scanning speed for t_3 is then set such that the t_3 delay between consecutive shots with the same t_1 delay and phase meets the Nyquist sampling criteria. For IR144, the t_1 delay was scanned from 0 to 102 fs in 6 fs steps in the partially rotating frame using a reference wavelength of 850 nm and the t_3 delay was scanned around time 0 for a total of 1.1 mm of stage travel at a speed of 0.4 mm/s (corresponding to ~-30 fs < t_3 < 30 fs). For bacteriochlorophyll *a*, the t_1 delay was scanned from 0 to 96 fs in 6 fs steps using a reference wavelength of 880 nm and the t_3 delay was scanned for a total of 2.8 mm of stage travel at a speed of 0.48 mm/s (corresponding to ~-80 fs < t_3 < 80 fs).

2.3 TWINS reproducibility, calibration and phasing

Since we continuously scan the t_3 axis, the movement of the TWINS stage is not synchronized with the data collection and the t_3 axis is not identical for every scan. Nevertheless, the time-domain data can still be acquired reproducibly, which is demonstrated in Figure 3 where we show a measurement of the linear autocorrelation trace of the white light continuum probe. Overall, the 100 individual scans line up well with the averaged scan. Without the use of any position tracking techniques, the standard deviation of the time jitter of the 100 scans is 1.83 shots, which corresponds to ~0.09 fs for a scanning speed of 1 mm/s.

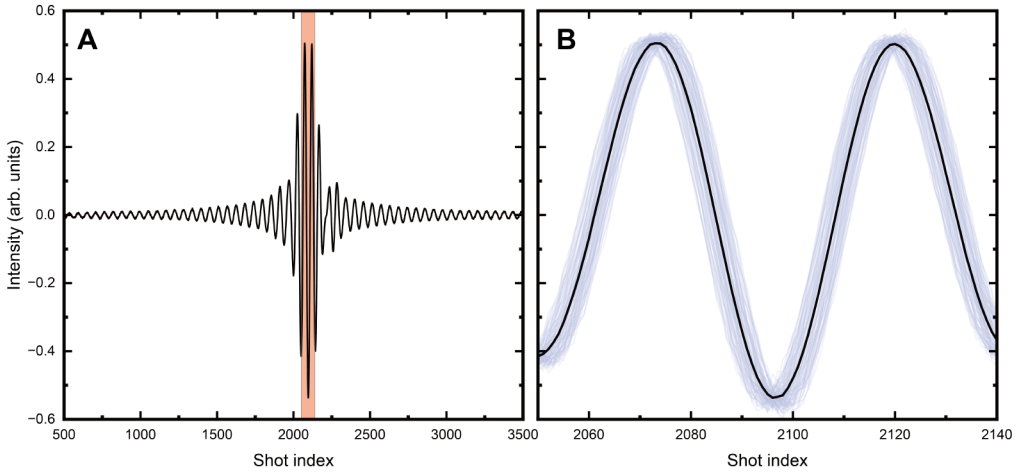

Fig. 3. (a) The averaged time-domain linear autocorrelation trace of the white light continuum probe used in the bacteriochlorophyll *a* experiment of 100 scans, measured by scanning the TWINS stage. (b) Zooming into the shaded area (orange) around the center of the autocorrelation in (a). The light gray curves refer to the 100 repetitions of individual scans. The black curve refers to the average of the 100 scans. The scanning speed of the TWINS stage is set at 1 mm/s. Note that in linear measurements the TWINS can be scanned much faster than in 2D experiments since the t_1 scan and phase-cycling of the pump pulse pair are not needed. The standard deviation of the time jitter is 1.83 shots, which corresponds to ~0.09 fs at the current scanning speed.

The calibration of the probe frequency axis is performed by measuring the spectral interferogram of the probe pulse pair while scanning t_3.[49, 55] From our experience, the calibration is robust enough to be performed separately from the actual experiment, and recalibration is only necessary when there is a major alignment change to the TWINS interferometer. To start, we block the pump beam, remove the sample, and couple the probe beam into a spectrometer. The spectral interferogram as a function of t_3 is collected by continuously scanning the TWINS interferometer at a predefined speed (1 mm/s). As displayed in Figure 4 (A), the linear autocorrelation trace of each probe wavelength is plotted against the shot index (sampling time). After performing a Fourier transform along the shot index axis, we can locate a well-defined peak on the pseudo-frequency axis for each probe wavelength, which establishes a mapping between the pseudo-frequency and the real frequency. We fit the correlation of frequencies to a 3rd order polynomial function, as displayed in Figure 4 (B). The relative fitting error is consistently below 0.1% for the probe frequency range of interest, demonstrating the high accuracy of this method. As proof of validity, Figure 7 (B) demonstrates the good agreement between the linear absorption spectrum of bacteriochlorophyll *a* in ethanol measured with a UV-Visible absorption spectrometer (Genesys 10, Thermo Electron Corporation) and the properly calibrated linear fluorescence excitation spectrum measured using the TWINS interferometer.

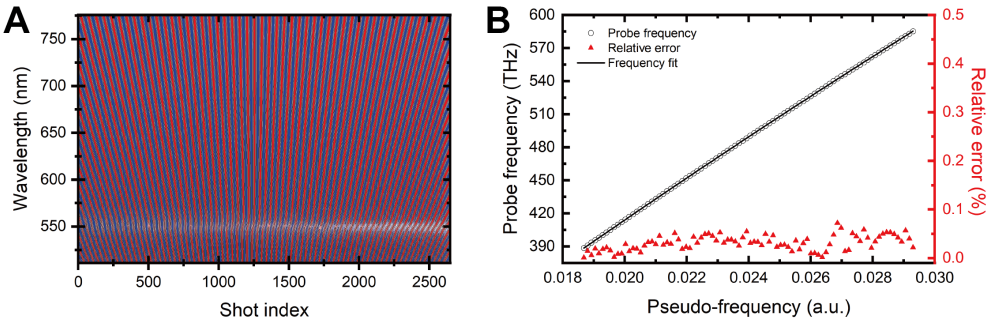

Fig. 4. (a) Spectral interferogram. (b) Calibration curve and relative fitting error.

The pseudo-frequency depends on the TWINS scanning speed and the data sampling rate. However, it is worth emphasizing that in an actual experiment the TWINS scanning speed can be different from the calibration speed. Additionally, as described in the previous section, the effective sampling rate along the t_3 axis varies according to the choice of the total number of t_1 steps and the number of phase-cycling/chopping cases used. To ensure proper calibration of the probe frequency, the pseudo-frequency axis defined in the actual experiment differs by a calculated scaling factor (the ratio of the experiment speed to the calibration speed). Applying the fitting results to the modified pseudo-frequency axis gives us the properly calibrated probe frequency axis.

Time zero is precisely known for t_1 so the acquired 2D spectra do not need to be phased along the pump axis, whereas it is not precisely known for t_3 so it is necessary to phase the spectra along the probe axis to properly separate rephasing and non-rephasing signals and avoid phase-twisted lineshapes. Determining $t_3 = 0$ can be performed using the linear fluorescence excitation signal from the probe, either using the approach of Helbing and Hamm,[56] as used by the Cerullo group [49], or as we have demonstrated previously. [43] We adopt the latter approach, where the time domain signals $[S_{NL+Lin,pumps}(t_1, T, t_3), S_{Lin,probe}(t_1, T, t_3)]$ are Fourier transformed into the frequency domain $[S_{NL+Lin,pumps}(\omega_1, T, \omega_3), S_{Lin,probe}(\omega_1, T, \omega_3)]$. The spectral phase $\Phi(\omega_3)$ is determined from $S_{Lin,probe}(\omega_1 = 0, T, \omega_3)$. To locate $t_3 = 0$ and correct timing errors due to the stage motion, we compute: $S'_{NL+Lin,pumps}(\omega_1, T, \omega_3) = S_{NL+Lin,pumps}(\omega_1, T, \omega_3) * e^{-i\Phi(\omega_3)}$. Finally, $S'_{NL+Lin,pumps}(\omega_1, T, \omega_3)$ is Fourier transformed back into the time domain, resulting in the signal with the correct t_3 axis: $S'_{NL+Lin,pumps}(t_1, T, t_3)$. The final phased spectra are obtained upon Fourier transform of the positive quadrant of the time domain data: $S'_{NL+Lin,pumps}(t_1 \geq 0, T, t_3 \geq 0)$.

Results and Discussion

3.1 IR144

To demonstrate the broadband F-2DES method, we first measured IR144 (Exciton) in ethanol (Sigma Aldrich). IR144 was dissolved into ethanol to a final concentration with an optical density (OD) of 0.2 (1 mm pathlength). The linear absorption spectrum of IR144 along with the corresponding pump and probe spectra are shown in Figure 5 (A). IR144 has a single broad absorption feature peaking at 754 nm. The pump excites a narrow portion of the broad absorption, whereas the probe covers the entire absorption band.

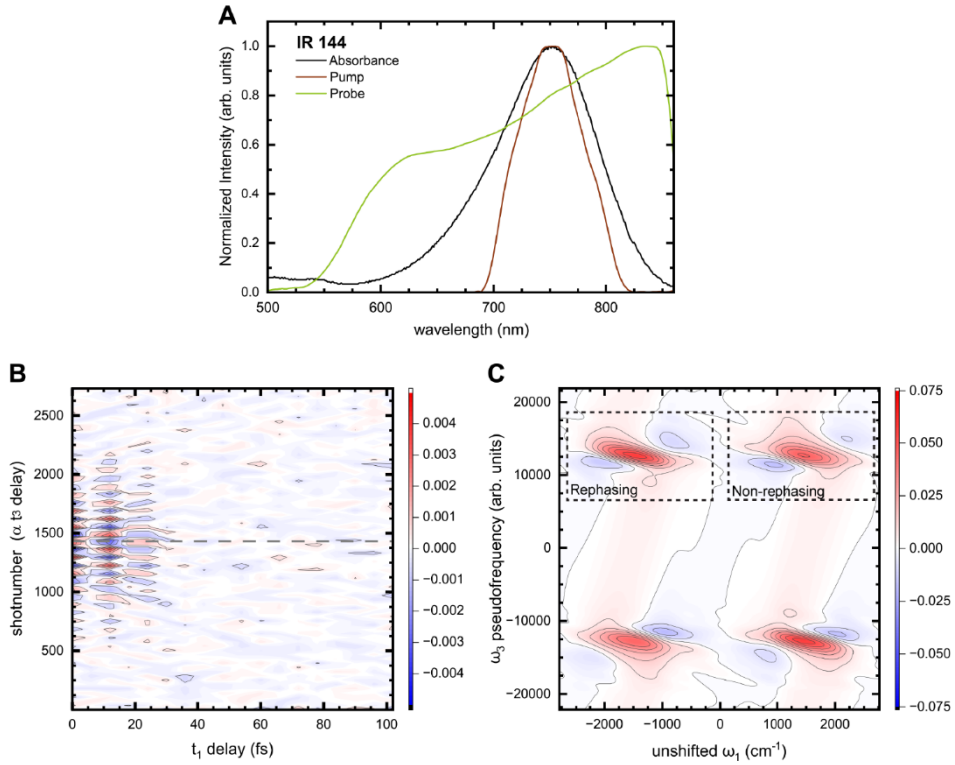

Fig. 5. (A) The IR144 absorption (black), pump (orange) and probe (green) spectrum. (B) Time-domain nonlinear signals of IR144. (C) Phased frequency-domain nonlinear signals of IR144, with the rephasing and non-rephasing signals clearly separated in frequency space.

The resulting time domain nonlinear signals extracted from the linear combination of the cases described in section 2.2 are shown in Figure 5 (B). The time domain data is symmetric around time zero in the t_3 axis (shot number ~2862), while t_1 is only scanned in the positive direction. The data shows clear dependence on both t_1 and t_3 with the signal decaying away from the origin. The symmetric scanning of t_3 enables easy determination of $t_3 = 0$ from the linear interferogram. After the Fourier transform along both the t_1 and t_3 axes, the nonlinear signals in the frequency domain are visualized in Figure 5 (C), where the rephasing and nonrephasing signals appear in different quadrants due to their differently-signed coherence frequencies during t_1.[57] The pump-probe signals appear at $(0,\pm\omega_3)$ and/or $(\pm\omega_1, 0)$ depending on the time ordering of the pump and probe pulses, whereas the rephasing and non-rephasing are at $(-\omega_1, \omega_3)$ and (ω_1, ω_3) respectively. The pump-probe signals are suppressed relative to the 2D signals during the phasing procedure, so they do not appear in Figure 5 (C). The additional two signals are the conjugates of the rephasing and non-rephasing. By carefully selecting the lock-wavelength for the partially rotating frame, the number of t_1 points needed for the Nyquist sampling criteria can be minimized while ensuring the signals are well separated in the frequency domain.

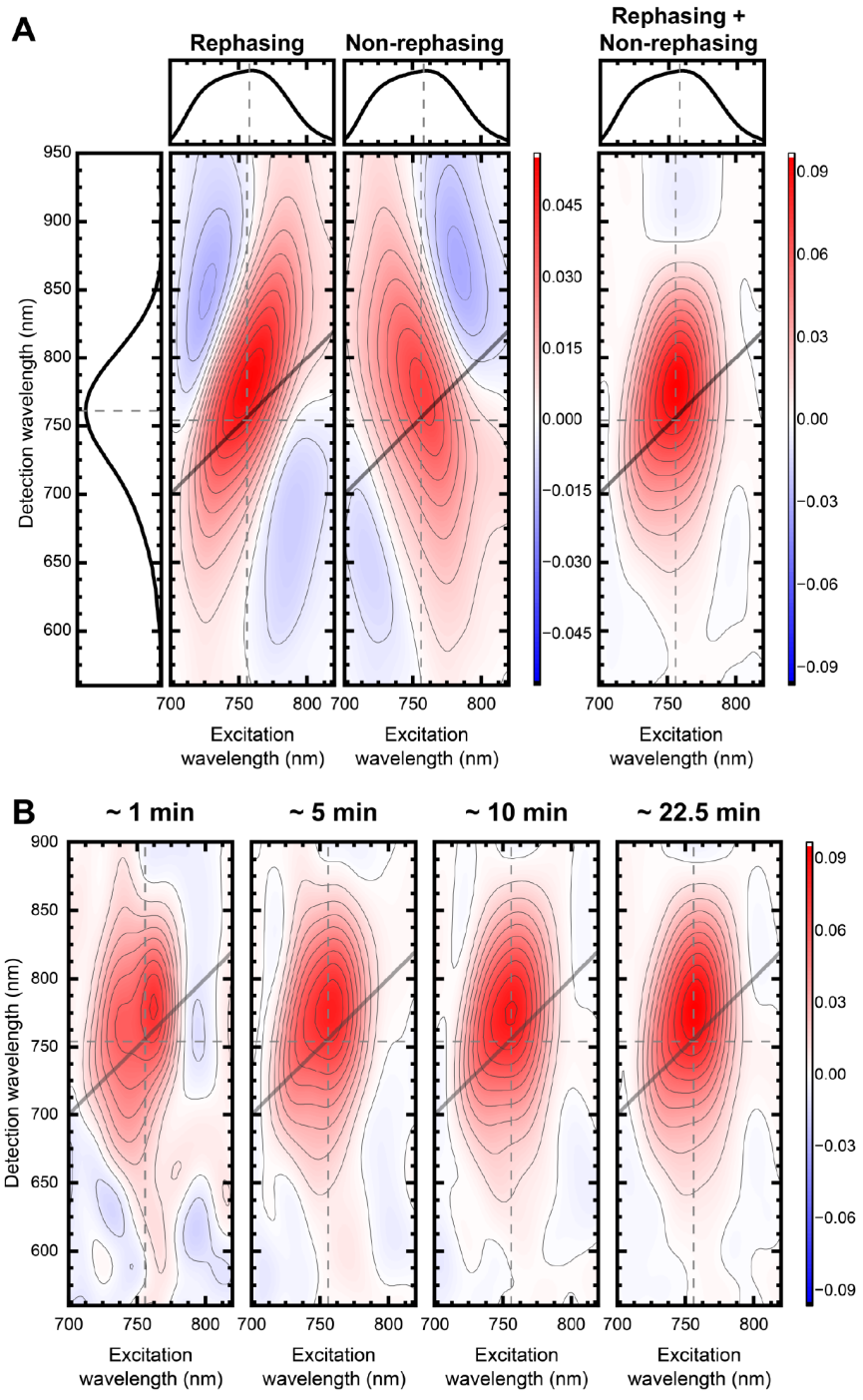

Fig. 6. (A) The rephasing, non-rephasing and absorptive spectra of IR144in ethanol at $T = 2$ ps, with the corresponding linear fluorescence excitation spectra from the pump and the probe shown alongside the excitation and detection axes respectively. Due to the chirp of the probe, the waiting time delay T is only for one certain frequency. (B) Comparison of the absorptive spectra with different data acquisition time.

As seen in Figure 6 (A), the rephasing and non-rephasing signals exhibit broad spectral features roughly along the diagonal and anti-diagonal respectively with the expected

characteristic lineshapes. At T = 2 ps, the rephasing + non-rephasing (absorptive) spectrum shows a broad response across the detection axis with a clear Stokes shift. Note that the response is all positive, corresponding to the GSB and SE, with no apparent ESA signal, highlighting the ability of F-2DES to suppress ESA signals. We note that the F-2DES spectral lineshapes are likely influenced by the chirp of the continuum probe, which could be post-corrected as has been done previously in coherent 2DES measurements.[58] In Figure 6 (B), we compare the absorptive spectra with different data acquisition times. The signal-to-noise ratio improves dramatically in the first ~10 minutes of data acquisition. Further averaging up to ~45 minutes (250 round trips of t_3 scanning) continues to offer some improvement.

3.2 Bacteriochlorophyll a

To demonstrate the ability of broadband F-2DES to probe multiple electronic transitions we study bacteriochlorophyll *a,* a pigment found in the photosynthetic antennas and reaction centers of many photosynthetic bacteria.[59] Bacteriochlorophyll *a* has electronic absorptions in the Q_x and Q_y bands at 600 nm and 780 nm, respectively, with Q_y displaying a prominent vibronic shoulder of comparable oscillator strength to Q_x. The pump excites the Q_y band plus the edge of the vibronic shoulder while the probe spans the Q_x and Q_y regions. The sample used in this experiment was prepared by dissolving bacteriochlorophyll *a* (*R. Sphaeroides,* Fisher Scientific) in nitrogen purged ethanol to an OD of 0.18 (0.4 mm pathlength). The linear absorption spectrum of bacteriochlorophyll *a* is presented in Figure 7 (A), along with the corresponding pump and probe spectra used in the experiment.

The resulting 2D signals are shown in Figure 7 (C), where we plot the rephasing, non-rephasing and absorptive spectra for $T \sim 0$ ps. Due to the chirp of the probe, the waiting time delay T is in reference to the absorption frequency of the Q_x band. Given the weak oscillator strength of the Q_x band and the vibronic shoulder, as well as the low intensity of the probe, a large number of averages is needed to obtain a decent signal-to-noise ratio. Each set of spectra for a single T delay took roughly 5 hours (1500 round trips of t_3 scanning). Apart from the dominant diagonal Q_y feature, we also observe cross-peaks between Q_y and the vibronic shoulder, and Q_y and Q_x, respectively. At $T \sim 0$ ps, the cross-peak between the Q_y and the vibronic shoulder as well as between Q_y and Q_x are evident in all three spectra. Improvements to the signal-to-noise ratio could be made by increasing the probe power and fully compressing the probe. For example, the use of a continuum probe generated by a hollow-core fiber and compressed with chirped mirrors would enable higher signal levels by using higher probe power. Asymmetric scanning of t_3 would also considerably reduce the data acquisition time.

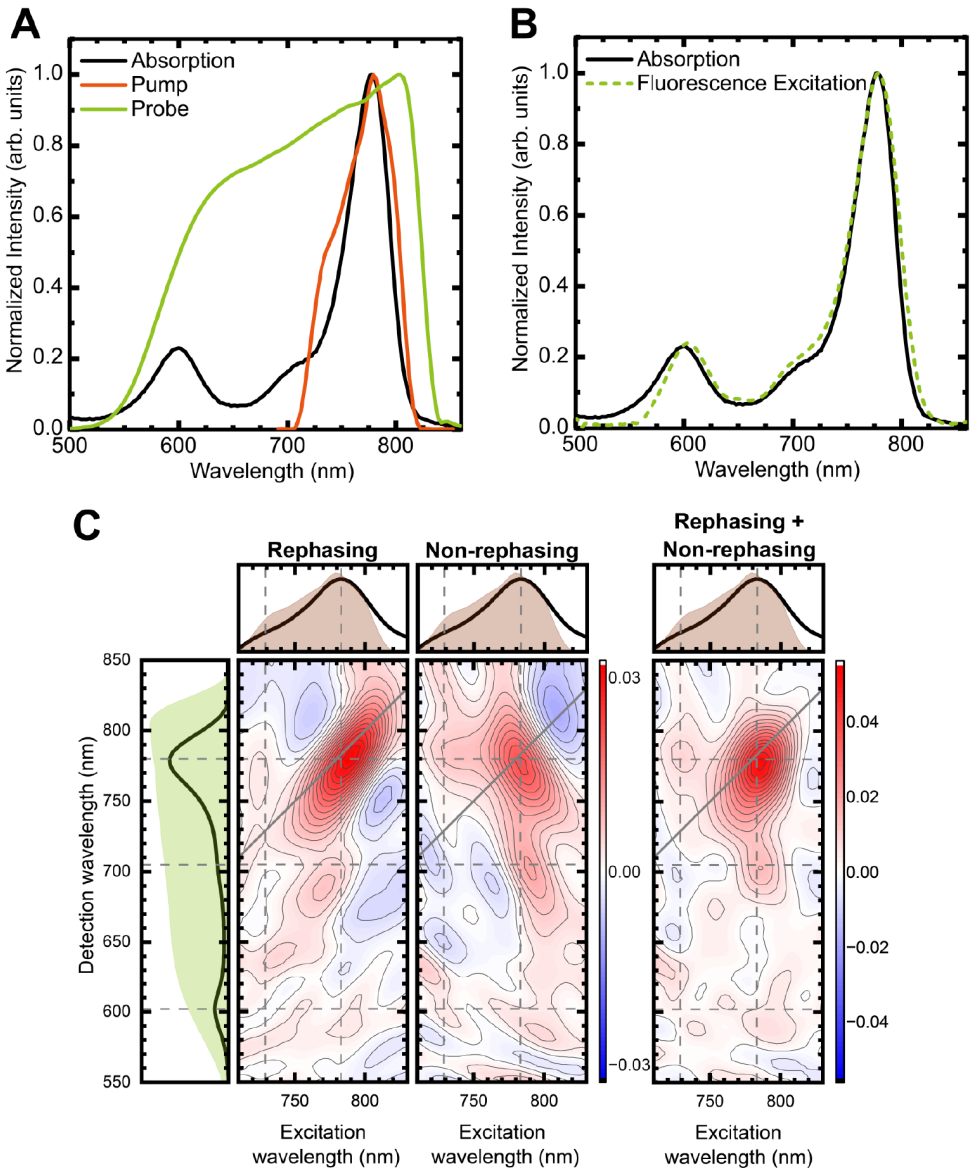

Fig. 7. (A) Bacteriochlorophyll *a* in ethanol absorption spectrum (black) with pump (orange) and probe (green) spectra used in the experiment. The main absorption featuresare the Q_x band at 600 nm and the Q_y band at 780 nm, as well as a vibronic shoulder at 720 nm. (B) The comparison between the absorption spectrum measured with a UV-Visible spectrometer and the properly calibrated linear fluorescence excitation spectrum measured using the TWINS interferometer. The spectra show good agreement, validating the TWINS calibration procedure discussed in section 2.3. Note that the slight mismatch at the Q_x peak is aresult of the probe spectral shape and does not impair the accuracy of the calibration result. (C) The rephasing, non-rephasing and absorptive spectra of bacteriochlorophyll *a* at $T \sim 0$ ps, with the corresponding linear fluorescence excitation spectra from the pump and the probe. Due to the chirp of the probe, the waiting time delay T is in reference to only the absorption frequency of the Q_x band. The vertical dashed lines label the Qy peak and the vibronic shoulder in the excitation axis, while the horizontal dashed lines label all three absorption features in the detection axis. The 2D spectra ~5 hours to acquire.

3. Conclusion and Outlook

In summary, we have demonstrated broadband F-2DES by combining a pulse-shaper for the pump pulses with a birefringent interferometer for the probe pulses. To separate out the nonlinear signals of interest we employ a combination of phase-cycling and frequency filtering. Given the utility of coherent 2DES with a white light probe in providing insights into systems with complex and congested spectra,[5, 19, 60-63] broadband F-2DES has exciting potential with the advantage of reducing dominant ESA signals. In our current implementation, the white light probe has a large temporal chirp, so the waiting time (T) is wavelength dependent, therefore further compression or chirp correction [58] is necessary to extract any dynamics. The ratio of nonlinear to linear signal could be improved by moving from the pump-probe geometry to the fully collinear geometry. However, the theoretical maximum throughput of the TWINS interferometer is half due to the final polarizer so combining the pump and probe with a beam splitter would result in additional losses, lowering the probe energy even further. With an alternative method of continuum white light generation such as hollow core fiber generation, higher probe power can be achieved. Data acquisition times could be reduced with asymmetric scanning of t_3.

Each of the three F-2DES implementations (phase-modulation via MZ interferometers, phase-cycling via pulse-shaper, broadband via pulse-shaper and birefringent interferometer) have advantages and disadvantages. Depending on the system of interest and desired experiments, the best method will vary. The phase-modulation via MZ interferometer method offers fast signal collection and good signal-to-noise ratios given the high repetition rates of the lasers used (250 kHz – 80 MHz). It is also easily coupled with a microscope and can access a long range of waiting time delays. However, this method is only compatible with high repetition rate lasers that cannot study long-lived species and have lower pulse energies. The bandwidth of the experiment is also limited by the acousto-optic modulators that perform the phase-modulation. The phase-cycling via pulse-shaper method offers fine and precise control of the time delays, which is useful in measuring coherences in the waiting time. Pulse-shaper methods are compatible with low repetition rate lasers capable of studying long-lived species. However, the bandwidth and range of accessible waiting times are limited by the size of the acousto-optic crystal in the pulse-shaper. The maximum T delay is 6-8 ps depending on the wavelength, but it is coupled to the bandwidth throughput of the pulse-shaper so the maximum waiting time delay for the excitation spectrum used in this study would be ~2 ps. In both previously described methods, the use of acousto-optic crystals limited the bandwidth. By generating the probe pulses with the TWINS interferometer, we were able to remove the acousto-optic crystal from two of the four pulses needed for the experiment and use a white light continuum probe. Compared to the fully pulse-shaper method, the TWIZZLER method also allows long waiting times to be accessed. Although the TWINS interferometer enables broadband throughput, the beam still travels through a lot of material, so the temporal chirp needs to be accounted for with precompensation (*i.e.,* chirped mirrors or prism compressor) or chirp correction in the analysis. We note that Tiwari and coworkers recently reported the use of TWINS for a continuum pump pulse pair in coherent 2DES.[64]

Funding. S.S., M.Z. and J.P.O gratefully acknowledge the support of the National Science Foundation through Grant #PHY-1914608. J.P.O and A.J. gratefully acknowledge support from the AFOSR Biophysics program under Grant No FA9550-18-1-0343.

Disclosures. The authors declare no conflicts of interest.

Data availability. Data underlying the results presented in this paper are not publicly available at this time but may be obtained from the authors upon reasonable request.

References

1. D. M. Jonas, "Two-Dimensional Femtosecond Spectroscopy," Annual Review of Physical Chemistry **54**, 425-463 (2003).
2. E. Fresch, F. V. A. Camargo, Q. Shen, C. C. Bellora, T. Pullerits, G. S. Engel, G. Cerullo, and E. Collini, "Two-dimensional electronic spectroscopy," Nature Reviews Methods Primers **3**, 84 (2023).
3. T. Brixner, J. Stenger, H. M. Vaswani, M. Cho, R. E. Blankenship, and G. R. Fleming, "Two-dimensional spectroscopy of electronic couplings in photosynthesis," Nature **434**, 625-628 (2005).
4. D. Paleček, P. Edlund, S. Westenhoff, and D. Zigmantas, "Quantum coherence as a witness of vibronically hot energy transfer in bacterial reaction center," Science Advances **3**, e1603141 (2017).
5. H. H. Nguyen, Y. Song, E. L. Maret, Y. Silori, R. Willow, C. F. Yocum, and J. P. Ogilvie, "Charge separation in the photosystem II reaction center resolved by multispectral two-dimensional electronic spectroscopy," Science Advances **9**, eade7190 (2023).
6. E. E. Ostroumov, R. M. Mulvaney, R. J. Cogdell, and G. D. Scholes, "Broadband 2D Electronic Spectroscopy Reveals a Carotenoid Dark State in Purple Bacteria," Science **340**, 52-56 (2013).
7. E. Thyrhaug, R. Tempelaar, M. J. P. Alcocer, K. Žídek, D. Bína, J. Knoester, T. L. C. Jansen, and D. Zigmantas, "Identification and characterization of diverse coherences in the Fenna–Matthews–Olson complex," Nature Chemistry **10**, 780-786 (2018).
8. A. Niedringhaus, V. R. Policht, R. Sechrist, A. Konar, P. D. Laible, D. F. Bocian, D. Holten, C. Kirmaier, and J. P. Ogilvie, "Primary processes in the bacterial reaction center probed by two-dimensional electronic spectroscopy," Proceedings of the National Academy of Sciences **115**, 3563-3568 (2018).
9. J. Lim, D. Paleček, F. Caycedo-Soler, C. N. Lincoln, J. Prior, H. Von Berlepsch, S. F. Huelga, M. B. Plenio, D. Zigmantas, and J. Hauer, "Vibronic origin of long-lived coherence in an artificial molecular light harvester," Nature Communications **6**, 7755 (2015).
10. E. Meneghin, F. Biscaglia, A. Volpato, L. Bolzonello, D. Pedron, E. Frezza, A. Ferrarini, M. Gobbo, and E. Collini, "Biomimetic Nanoarchitectures for Light Harvesting: Self-Assembly of Pyropheophorbide-Peptide Conjugates," The Journal of Physical Chemistry Letters **11**, 7972-7980 (2020).
11. K. W. Stone, D. B. Turner, K. Gundogdu, S. T. Cundiff, and K. A. Nelson, "Exciton−Exciton Correlations Revealed by Two-Quantum, Two-Dimensional Fourier Transform Optical Spectroscopy," Accounts of Chemical Research **42**, 1452-1461 (2009).
12. D. Karaiskaj, A. D. Bristow, L. Yang, X. Dai, R. P. Mirin, S. Mukamel, and S. T. Cundiff, "Two-Quantum Many-Body Coherences in Two-Dimensional Fourier-Transform Spectra of Exciton Resonances in Semiconductor Quantum Wells," Physical Review Letters **104**, 117401 (2010).
13. S. D. Park, D. Baranov, J. Ryu, B. Cho, A. Halder, S. Seifert, S. Vajda, and D. M. Jonas, "Bandgap Inhomogeneity of a PbSe Quantum Dot Ensemble from Two-Dimensional Spectroscopy and Comparison to Size Inhomogeneity from Electron Microscopy," Nano Letters **17**, 762-771 (2017).
14. Y. Song, S. N. Clafton, R. D. Pensack, T. W. Kee, and G. D. Scholes, "Vibrational coherence probes the mechanism of ultrafast electron transfer in polymer–fullerene blends," Nature Communications **5**, 4933 (2014).
15. Y. Song, X. Liu, Y. Li, H. H. Nguyen, R. Duan, K. J. Kubarych, S. R. Forrest, and J. P. Ogilvie, "Mechanistic Study of Charge Separation in a Nonfullerene Organic Donor–Acceptor Blend Using Multispectral Multidimensional Spectroscopy," The Journal of Physical Chemistry Letters **12**, 3410-3416 (2021).
16. J. A. Myers, K. L. Lewis, P. F. Tekavec, and J. P. Ogilvie, "Two-color two-dimensional Fourier transform electronic spectroscopy with a pulse-shaper," Opt. Express **16**, 17420 (2008).
17. P. F. Tekavec, J. A. Myers, K. L. M. Lewis, and J. P. Ogilvie, "Two-dimensional electronic spectroscopy with a continuum probe," Opt. Lett. **34**, 1390-1392 (2009).
18. A. Konar, R. Sechrist, Y. Song, V. R. Policht, P. D. Laible, D. F. Bocian, D. Holten, C. Kirmaier, and J. P. Ogilvie, "Electronic Interactions in the Bacterial Reaction Center Revealed by Two-Color 2D Electronic Spectroscopy," The Journal of Physical Chemistry Letters **9**, 5219-5225 (2018).
19. Y. Song, R. Sechrist, H. H. Nguyen, W. Johnson, D. Abramavicius, K. E. Redding, and J. P. Ogilvie, "Excitonic structure and charge separation in the heliobacterial reaction center probed by multispectral multidimensional spectroscopy," Nature Communications **12**, 2801 (2021).
20. Y. Yoneda, E. A. Arsenault, S. Yang, Jr., K. Orcutt, M. Iwai, and G. R. Fleming, "The initial charge separation step in oxygenic photosynthesis," Nature Communications **13**, 2275 (2022).
21. K. Zakutauskaitė, M. Mačernis, H. H. Nguyen, J. P. Ogilvie, and D. Abramavičius, "Extracting the excitonic Hamiltonian of a chlorophyll dimer from broadband two-dimensional electronic spectroscopy," The Journal of Chemical Physics **158**, 015103 (2023).
22. W. Wagner, C. Li, J. Semmlow, and W. S. Warren, "Rapid phase-cycled two-dimensional optical spectroscopy in fluorescence and transmission mode," Opt. Express **13**, 3697-3706 (2005).
23. P. F. Tekavec, G. A. Lott, and A. H. Marcus, "Fluorescence-detected two-dimensional electronic coherence spectroscopy by acousto-optic phase modulation," The Journal of Chemical Physics **127**, 214307 (2007).
24. S. Draeger, S. Roeding, and T. Brixner, "Rapid-scan coherent 2D fluorescence spectroscopy," Opt. Express **25**, 3259-3267 (2017).
25. A. K. De, D. Monahan, J. M. Dawlaty, and G. R. Fleming, "Two-dimensional fluorescence-detected coherent spectroscopy with absolute phasing by confocal imaging of a dynamic grating and 27-step phase-cycling," The Journal of Chemical Physics **140**, 194201 (2014).

26. V. Tiwari, Y. A. Matutes, A. Konar, Z. Yu, M. Ptaszek, D. F. Bocian, D. Holten, C. Kirmaier, and J. P. Ogilvie, "Strongly coupled bacteriochlorin dyad studied using phase-modulated fluorescence-detected two-dimensional electronic spectroscopy," Opt. Express **26**, 22327 (2018).
27. G. A. Lott, A. Perdomo-Ortiz, J. K. Utterback, J. R. Widom, A. Aspuru-Guzik, and A. H. Marcus, "Conformation of self-assembled porphyrin dimers in liposome vesicles by phase-modulation 2D fluorescence spectroscopy," Proceedings of the National Academy of Sciences **108**, 16521-16526 (2011).
28. P. Malý, J. Lüttig, S. Mueller, M. H. Schreck, C. Lambert, and T. Brixner, "Coherently and fluorescence-detected two-dimensional electronic spectroscopy: direct comparison on squaraine dimers," Physical Chemistry Chemical Physics **22**, 21222-21237 (2020).
29. D. Heussman, J. Kittell, P. H. Von Hippel, and A. H. Marcus, "Temperature-dependent local conformations and conformational distributions of cyanine dimer labeled single-stranded–double-stranded DNA junctions by 2D fluorescence spectroscopy," The Journal of Chemical Physics **156**, 045101 (2022).
30. V. Tiwari, Y. A. Matutes, A. T. Gardiner, T. L. C. Jansen, R. J. Cogdell, and J. P. Ogilvie, "Spatially-resolved fluorescence-detected two-dimensional electronic spectroscopy probes varying excitonic structure in photosynthetic bacteria," Nature Communications **9**, 4219 (2018).
31. K. J. Karki, J. Chen, A. Sakurai, Q. Shi, A. T. Gardiner, O. Kühn, R. J. Cogdell, and T. Pullerits, "Before Förster. Initial excitation in photosynthetic light harvesting," Chemical Science **10**, 7923-7928 (2019).
32. T. Kunsel, V. Tiwari, Y. A. Matutes, A. T. Gardiner, R. J. Cogdell, J. P. Ogilvie, and T. L. C. Jansen, "Simulating Fluorescence-Detected Two-Dimensional Electronic Spectroscopy of Multichromophoric Systems," The Journal of Physical Chemistry B **123**, 394-406 (2019).
33. O. Kühn, T. Mančal, and T. Pullerits, "Interpreting Fluorescence Detected Two-Dimensional Electronic Spectroscopy," The Journal of Physical Chemistry Letters **11**, 838-842 (2020).
34. L. Bolzonello, M. Bruschi, B. Fresch, and N. F. van Hulst, "Nonlinear Optical Spectroscopy of Molecular Assemblies: What Is Gained and Lost in Action Detection?," The Journal of Physical Chemistry Letters, 11438-11446 (2023).
35. P. Malý, and T. Mančal, "Signatures of Exciton Delocalization and Exciton–Exciton Annihilation in Fluorescence-Detected Two-Dimensional Coherent Spectroscopy," The Journal of Physical Chemistry Letters **9**, 5654-5659 (2018).
36. K. J. Karki, J. R. Widom, J. Seibt, I. Moody, M. C. Lonergan, T. Pullerits, and A. H. Marcus, "Coherent two-dimensional photocurrent spectroscopy in a PbS quantum dot photocell," Nature Communications **5**, 5869 (2014).
37. S. Mueller, J. Lüttig, L. Brenneis, D. Oron, and T. Brixner, "Observing Multiexciton Correlations in Colloidal Semiconductor Quantum Dots via Multiple-Quantum Two-Dimensional Fluorescence Spectroscopy," ACS Nano **15**, 4647-4657 (2021).
38. M. Bruschi, F. Gallina, and B. Fresch, "Simulating action-2D electronic spectroscopy of quantum dots: insights on the exciton and biexciton interplay from detection-mode and time-gating," Physical Chemistry Chemical Physics **24**, 27645-27659 (2022).
39. I. Bargigia, E. Gutiérrez-Meza, D. A. Valverde-Chávez, S. R. Marques, A. R. Srimath Kandada, and C. Silva, "Identifying incoherent mixing effects in the coherent two-dimensional photocurrent excitation spectra of semiconductors," The Journal of Chemical Physics **157**, 204202 (2022).
40. P. Grégoire, A. R. Srimath Kandada, E. Vella, C. Tao, R. Leonelli, and C. Silva, "Incoherent population mixing contributions to phase-modulation two-dimensional coherent excitation spectra," The Journal of Chemical Physics **147**, 114201 (2017).
41. A. A. S. Kalaee, F. Damtie, and K. J. Karki, "Differentiation of True Nonlinear and Incoherent Mixing of Linear Signals in Action-Detected 2D Spectroscopy," The Journal of Physical Chemistry A **123**, 4119-4124 (2019).
42. M. Bruschi, L. Bolzonello, F. Gallina, and B. Fresch, "Unifying Nonlinear Response and Incoherent Mixing in Action-2D Electronic Spectroscopy," The Journal of Physical Chemistry Letters **14**, 6872-6879 (2023).
43. D. Agathangelou, A. Javed, F. Sessa, X. Solinas, M. Joffre, and J. P. Ogilvie, "Phase-modulated rapid-scanning fluorescence-detected two-dimensional electronic spectroscopy," The Journal of Chemical Physics **155**, 094201 (2021).
44. A. Sahu, V. N. Bhat, S. Patra, and V. Tiwari, "High-sensitivity fluorescence-detected multidimensional electronic spectroscopy through continuous pump–probe delay scan," The Journal of Chemical Physics **158**, 024201 (2023).
45. E. M. Grumstrup, S.-H. Shim, M. A. Montgomery, N. H. Damrauer, and M. T. Zanni, "Facile collection of two-dimensional electronic spectra using femtosecond pulse-shaping technology," Opt. Express **15**, 16681-16689 (2007).
46. H.-S. Tan, "Theory and phase-cycling scheme selection principles of collinear phase coherent multi-dimensional optical spectroscopy," The Journal of Chemical Physics **129**, 124501 (2008).
47. S. Goetz, D. Li, V. Kolb, J. Pflaum, and T. Brixner, "Coherent two-dimensional fluorescence micro-spectroscopy," Opt. Express **26**, 3915-3925 (2018).
48. D. Brida, C. Manzoni, and G. Cerullo, "Phase-locked pulses for two-dimensional spectroscopy by a birefringent delay line," Opt. Lett. **37**, 3027-3029 (2012).
49. J. Réhault, M. Maiuri, A. Oriana, and G. Cerullo, "Two-dimensional electronic spectroscopy with birefringent wedges," Review of Scientific Instruments **85**, 123107 (2014).
50. R. Borrego-Varillas, A. Oriana, L. Ganzer, A. Trifonov, I. Buchvarov, C. Manzoni, and G. Cerullo, "Two-dimensional electronic spectroscopy in the ultraviolet by a birefringent delay line," Opt. Express **24**, 28491 (2016).

51. J. Réhault, R. Borrego-Varillas, A. Oriana, C. Manzoni, C. P. Hauri, J. Helbing, and G. Cerullo, "Fourier transform spectroscopy in the vibrational fingerprint region with a birefringent interferometer," Opt. Express **25**, 4403 (2017).
52. A. Perri, B. E. Nogueira De Faria, D. C. T. Ferreira, D. Comelli, G. Valentini, F. Preda, D. Polli, A. M. De Paula, G. Cerullo, and C. Manzoni, "Hyperspectral imaging with a TWINS birefringent interferometer," Opt. Express **27**, 15956 (2019).
53. A. M. Siddiqui, G. Cirmi, D. Brida, F. X. Kärtner, and G. Cerullo, "Generation of <7 fs pulses at 800 nm from a blue-pumped optical parametric amplifier at degeneracy," Opt. Lett. **34**, 3592-3594 (2009).
54. S.-H. Shim, and M. T. Zanni, "How to turn your pump–probe instrument into a multidimensional spectrometer: 2D IR and Vis spectroscopiesvia pulse shaping," Phys. Chem. Chem. Phys. **11**, 748-761 (2009).
55. L. Lepetit, G. Chériaux, and M. Joffre, "Linear techniques of phase measurement by femtosecond spectral interferometry for applications in spectroscopy," J. Opt. Soc. Am. B **12**, 2467-2474 (1995).
56. J. Helbing, and P. Hamm, "Compact implementation of Fourier transform two-dimensional IR spectroscopy without phase ambiguity," J. Opt. Soc. Am. B **28**, 171-178 (2011).
57. Z. Zhang, K. L. Wells, E. W. J. Hyland, and H.-S. Tan, "Phase-cycling schemes for pump–probe beam geometry two-dimensional electronic spectroscopy," Chemical Physics Letters **550**, 156-161 (2012).
58. K. L. M. L. Patrick A. Tekavec, Franklin D. Fuller, Jeffrey A. Myers, and Jennifer P. Ogilvie, "Toward Broad Bandwidth 2-D Electronic Spectroscopy: Correction of Chirp From a Continuum Probe," IEEE Journal of Selected Topics in Quantum Electronics **18**, 210-217 (2012).
59. R. E. Blankenship, *Molecular Mechanisms of Photosynthesis* (Wiley, 2002).
60. A. C. Jones, N. M. Kearns, J.-J. Ho, J. T. Flach, and M. T. Zanni, "Impact of non-equilibrium molecular packings on singlet fission in microcrystals observed using 2D white-light microscopy," Nature Chemistry **12**, 40-47 (2020).
61. A. Mandal, M. Chen, E. D. Foszcz, J. D. Schultz, N. M. Kearns, R. M. Young, M. T. Zanni, and M. R. Wasielewski, "Two-Dimensional Electronic Spectroscopy Reveals Excitation Energy-Dependent State Mixing during Singlet Fission in a Terrylenediimide Dimer," Journal of the American Chemical Society **140**, 17907-17914 (2018).
62. A. Mandal, J. D. Schultz, Y.-L. Wu, A. F. Coleman, R. M. Young, and M. R. Wasielewski, "Transient Two-Dimensional Electronic Spectroscopy: Coherent Dynamics at Arbitrary Times along the Reaction Coordinate," The Journal of Physical Chemistry Letters **10**, 3509-3515 (2019).
63. M. Son, A. Pinnola, S. C. Gordon, R. Bassi, and G. S. Schlau-Cohen, "Observation of dissipative chlorophyll-to-carotenoid energy transfer in light-harvesting complex II in membrane nanodiscs," Nature Communications **11**, 1295 (2020).
64. A. S. Thomas, V. N. Bhat, and V. Tiwari, "Rapid scan white light two-dimensional electronic spectroscopy with 100 kHz shot-to-shot detection," The Journal of Chemical Physics **159**, 244202 (2023).